

# Revisiting Reactor Anti-Neutrino 5 MeV Bump with $^{13}\text{C}$ Neutral-Current Interaction

Pouya Bakhti,<sup>1,\*</sup> Min-Gwa Park,<sup>1,†</sup> Meshkat Rajaei,<sup>1,‡</sup> Chang Sub Shin,<sup>2,3,4,§</sup> and Seodong Shin<sup>1,3,¶</sup>

<sup>1</sup>*Laboratory for Symmetry and Structure of the Universe, Department of Physics,  
Jeonbuk National University, Jeonju, Jeonbuk 54896, Korea*

<sup>2</sup>*Department of Physics and Institute of Quantum Systems,  
Chungnam National University, Daejeon 34134, Korea*

<sup>3</sup>*Center for Theoretical Physics of the Universe,  
Institute for Basic Science, Daejeon 34126, Korea*

<sup>4</sup>*Korea Institute for Advanced Study, Seoul 02455, Korea*

For the first time, we comprehensively examine the potential of neutrino-nucleus neutral current interactions with  $^{13}\text{C}$  to determine the origin of the 5-MeV bump in reactor antineutrino spectra observed through the inverse beta decay (IBD) process. This anomaly may be due to new physics, reactor antineutrino flux inaccuracies, or IBD systematics. The primary signal is the 3.685 MeV photon released during the de-excitation of  $^{13}\text{C}^*$  to its ground state, detectable in various liquid scintillator detectors. This interaction is most common for reactor antineutrinos within the energy range of the 5-MeV bump, providing unique sensitivity to its origins. Remarkably, we confirm the powerfulness of our proposal by completely ruling out a new physics scenario explaining the bump from the existing NEOS data. The main systematic challenge in distinguishing flux models is the accuracy of cross-section measurements; thus, minimizing these uncertainties is essential. Hence, we explore the potential of current and forthcoming experiments, including solar neutrino studies at JUNO, pion and muon decay-at-rest experiments at OscSNS, and isotope decay-at-rest studies at Yemilab, to obtain precise cross-section measurements. Additionally, we propose a novel method to track the time evolution of reactor isotopes by analyzing the  $^{13}\text{C}$  signal. This technique yields critical insights into the contributions of  $^{235}\text{U}$  and  $^{239}\text{Pu}$  to the observed bump, acting as a robust tool to differentiate between flux models and explore new physics explanations for the 5-MeV bump.

## I. INTRODUCTION.

Since its first discovery [1], reactor neutrinos have advanced our comprehension of the lepton sector. Notably, the KamLAND experiment confirmed the neutrino oscillation as the explanation for the solar neutrino problem [2]. Daya Bay [3], RENO [4], and Double Chooz [5] experiments measured a non-zero value of oscillation parameter  $\theta_{13}$ . This discovery has opened the possibility of CP violation in neutrino oscillation. Future reactor neutrino experiment JUNO [6] aims to determine the neutrino mass ordering and achieve sub-percent precision in measuring solar neutrino oscillation parameters, which can be complemented by the liquid scintillator counter at Korean new underground lab, Yemilab [7, 8], promising precise investigations into solar characteristics.

Probes of neutrino oscillation using reactor neutrinos necessitate accurate theoretical predictions of the neutrino flux. However, its calculation is very complicated and traces its origins to the early days subsequent to the first detection of neutrinos in the Cowan and Reines reactor experiment [1]. The Vogel model [9], employed as the standard flux model for two decades starting from the 1990s, relies on the conversion method and predicts reactor flux measurements based on the Institut Laue-Langevin (ILL) electron spectrum measurements [10, 11].

Interestingly, the actual neutrino fluxes measured in several short-baseline reactor neutrino experiments with varying fission fractions were smaller than the expected values, which has drawn more careful calculations, such as those by Mueller et al. [12] and Huber [13]. Nonethe-

less, the predicted fluxes still surpass the observations by about 6% corresponding to a  $3\sigma$  level discrepancy in the overall energy spectra, now dubbed as the reactor antineutrino anomaly (RAA) [14].

Moving the focus to a narrower prompt energy range of 4 to 6 MeV, the situation becomes more arduous. In contrast to the deficit in the overall flux, the observed data first reported by RENO [15], and then confirmed by other experiments such as Daya Bay [16], Double Chooz [5], NEOS [17], Neutrino-4 [18], and DANSS (preliminary) [19] at more than  $4\sigma$ . Moreover, STEREO [20] and PROSPECT [21], utilizing research reactors powered by 100%  $^{235}\text{U}$  fuel, have excluded the no 5 MeV bump scenario with more than  $3.5\sigma$  and  $2\sigma$  C.L. respectively. This anomaly is called the *5 MeV bump* [22].

Reactor electron anti-neutrinos are predominantly detected through the inverse beta decay (IBD) reaction, offering distinct advantages such as a large cross-section and a clear coincidence of the prompt positron annihilation and the delayed neutron capture  $\gamma$ -ray emission. The detection threshold for IBD is 1.8 MeV. The previously mentioned 5 MeV bump is observed from IBD, which means the positron energies peak around 5 MeV beyond all the theoretical expectation including the Huber-Mueller (HM) model. To further investigate its origin, whether it is coming from a miscalculation of the flux, new physics [23], or IBD systematic, employing another detection approach is advantageous. In this paper, for the first time, we propose to use the neutral current (NC) interaction of neutrinos with  $^{13}\text{C}$  isotope ubiquitous with mostly about 1.1 % abundance in the carbon-based liquid scintillator (LS) detectors to identify the 5 MeV bump al-

ternatively to the IBD. The interaction threshold is 3.685 MeV, resulting in the excitation of  $^{13}\text{C}$  nuclei to their first excited state. Then, a 3.685 MeV  $\gamma$ -ray emits from prompt de-excitation of  $^{13}\text{C}^*$  nuclei, creating a distinctive signal. Note that NC interactions are flavor blind and are not affected by neutrino oscillation parameter uncertainties. However, other types of interactions such as neutrino-electron elastic scattering (ES) and coherent elastic neutrino-nucleus scattering ( $\text{CE}\nu\text{NS}$ ), which benefit from low energy thresholds, suffer from large systematic uncertainty, and detecting signals above the background poses significant challenges rendering them less suitable for studying the 5 MeV bump. It is worth noting that CC and NC interactions of deuterons can be alternative methods in experiments with a sufficient quantity of heavy water [24].

The origin of the observed 5-MeV spectral bump may be attributed to new physics, inaccuracies in IBD systematics, or errors in flux calculations. In the context of new physics, the observed 5-MeV bump could be explained either by modifications to the flux — such as the production of new particles that decay into  $\bar{\nu}_e$ —or through mechanisms that do not alter the flux. In the first case, distinguishing this scenario from a standard model (SM) flux miscalculation using  $^{13}\text{C}$  events is not feasible. However, in the second case, such mechanisms would be distinguishable through the  $^{13}\text{C}$  signal. In this regard, we validate the effectiveness of our alternative channel by directly searching for the 3.685 MeV photon signal in the recent NEOS results, conclusively ruling out the new physics explanation of the 5-MeV bump such as the scenario involving a sterile neutrino with an additional  $\text{U}(1)$  gauge symmetry [23]. This conclusion arises from the fact that such a new physics scenario would predict a significant, sharp photon peak around 3.685 MeV, well above the background events, resulting from sterile neutrino scattering with  $^{13}\text{C}$  mediated by a light  $Z'$  boson. The absence of this peak in the existing data strongly disfavors this explanation.

In case that bump results from IBD systematics, measurements of the  $^{13}\text{C}$  flux are expected to align with flux models. As an example of IBD systematics, reconstructing prompt energy in liquid scintillators involves several complexities. The light yield demonstrates non-linearity with respect to the energy deposited by charged particles, primarily due to the quenching effect, as described by Birks' law [25, 26], and contributions from Cherenkov radiation. Furthermore, electronic readout systems may introduce additional non-linearity by inaccurately estimating the number of detected photoelectrons. Variations in detector response, depending on the event position, further exacerbate these challenges. Consequently, comprehensive calibration procedures are critical for accurate prompt energy reconstruction. To address the 5-MeV bump effectively and verify that it is not a systematic artifact, alternative methods, such as analyzing  $^{13}\text{C}$  events, are indispensable.

To assess the broader feasibility of our proposed chan-

nel beyond the specific scenario discussed, we perform a detailed analysis of background events and calculate the signal-to-background ratio required to differentiate between various reactor neutrino flux models. This analysis is presented in the appendix. Moreover, the most significant systematic uncertainty in differentiating reactor flux models arises from cross-section measurements. To address this issue, we explore the potential of current and future experiments—such as solar neutrino studies at JUNO, pion and muon decay-at-rest experiments at OscSNS, and isotope decay-at-rest studies at Yemilab—to achieve precise and accurate cross-section measurements. Additionally, we assess the feasibility of measuring the cross section under various reactor models to enhance our understanding and improve the reliability of flux model separation.

The structure of the paper is as follows. In Sec. II, we discuss the expected number of events for  $^{13}\text{C}$ . Section III examines a Beyond the Standard Model (BSM) scenario that addresses the 5-MeV bump using  $^{13}\text{C}$  events at NEOS. In Sec. IV, we provide a detailed analysis of the  $^{13}\text{C}$  cross-section measurement. Section V investigates the potential for differentiating reactor flux models and their application in detecting fission fraction evolution. Finally, our conclusions are presented in Sec. VI. The detailed explanations on the background analysis along with an experimental proposal realizing our goal are summarized in Appendix A .

## II. CROSS SECTION OF $^{13}\text{C}$ NC AND EXPECTED EVENTS.

In this section, we discuss the Cross section and expected signal events associated with  $^{13}\text{C}$  in carbon-based liquid scintillators.

The cross section for the neutral current interaction of neutrinos with  $^{13}\text{C}$  is given by [27]:

$$\sigma(E_\nu) = [a_1(E_\nu - Q) + a_2(E_\nu - Q)^2] \times 10^{-44} \text{cm}^2 \quad (1)$$

where  $Q = 3.685$  MeV is the energy threshold,  $a_1 = 0.122$ , and  $a_2 = 1.26$  are constants [28, 29]. Fig. 1 shows the cross section represented by the dashed green curve. Notice that for light nuclei such as  $^{13}\text{C}$ , there is a good agreement between theory and experiment. Hence, we display Fig. 1 assuming that the cross section uncertainty would follow the best theoretical calculations to the 1% level [30, 31] although its experimental measurement lacks so far. Following the solar neutrino flux observation proposals using the  $^{13}\text{C}$  NC interaction [31–33], we expect to measure the cross section within a few % level uncertainty in the near future as explained in Sec. IV.

In Fig. 1, we present the flux of reactor neutrinos with the dashed blue curve, assuming the HM model [12, 13] and considering the average fission fractions at near detector of RENO [37] as follows: 0.571 for  $^{235}\text{U}$ , 0.073 for

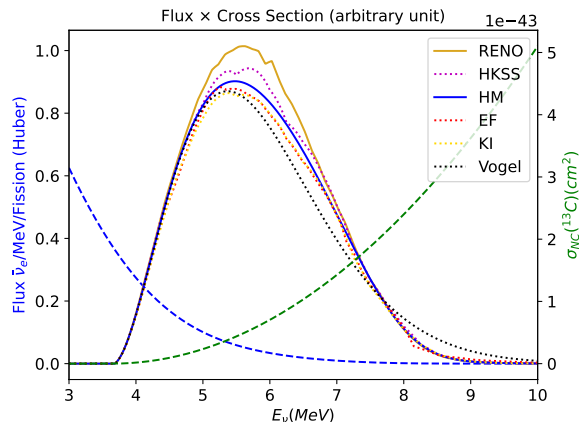


FIG. 1. The flux of reactor neutrinos based on the Huber-Mueller (HM) model is depicted by a dashed blue curve [12, 13]. The cross-section of NC  $\bar{\nu}_e - {}^{13}\text{C}$  is shown by a dashed green curve [27]. Additionally, the product of the reactor neutrino flux and the cross-section is evaluated across several reactor models, including HKSS [34], HM, EF [35], KI [36], and Vogel [9], and for the reconstructed flux from RENO [37]. These calculations assume identical fission fractions as reported for near detector of RENO [37].

${}^{238}\text{U}$ , 0.3 for  ${}^{239}\text{Pu}$ , and 0.056 for  ${}^{241}\text{Pu}$ . Other reactor models are not illustrated as they overlap with each other. Moreover, we show the product of the flux and the  $\bar{\nu}_e$  interaction cross-section with  ${}^{13}\text{C}$ , considering various flux models such as HM, Vogel [9], KI (Kurchatov Institute) [36], EF (Estienne-Fallot) [35], and HKSS (Hayen-Kostensalo-Severijns-Suhonen) [34], as well as the reconstructed number of events considering excess events at RENO [15]. For a review of different models, see [38, 39].

As demonstrated in Fig. 1, a significant number of events falls within the neutrino energy range of 4.5 to 7.5 MeV, coinciding with the 5 MeV bump anomaly. This interaction thus presents a novel opportunity to investigate the origin of the bump and possibly differentiate among reactor flux models, offering a new channel testing the phenomenon. The ratios of events for the Vogel, KI, EF, and HKSS models to HM model are 0.96, 0.96, 0.97, and 1.03, respectively [40]. Assuming all the excess events in the IBD measurements as reported in Ref. [39] are caused by a higher flux, the experimental events involving  ${}^{13}\text{C}$  will likely be 4% to 8% higher than predicted by the HM model. In the case of RENO [37], as demonstrated in Fig. 1, it is 12% higher than the EF or KI models which fit the RAA within about  $1\sigma$  level. Hence investigations identifying the origin of the 5 MeV bump rely on how much we can reduce the uncertainties in the current/future experiments.

We present the annual number of  ${}^{13}\text{C}$  events for various current or near-future reactor neutrino experiments in Table I. The number of events is directly proportional to reactor power and detector mass, and the inverse of the square of the baseline. Assuming the average fission

Experiments	P(GW)	m(t)	Baseline(m)	events/yr
Daya Bay (near/far)	17.4/17.4	80/80	578.7/1638	88/11
RENO (near/far)	16.4/16.4	16/16	420/1400	38/3.4
PROSPECT-II	3	4.8	25	491
JUNO-TAO	4.6	2.8	30	305
NEOS	2.8	1	24	103

TABLE I. A summary of power, mass, baseline and the expected number reactor  $\bar{\nu} {}^{13}\text{C}$  NC events for various experiments.

fraction reported by near detector of RENO [37] and employing the HM model, the annual number of  ${}^{13}\text{C}$  events in a commercial reactor is estimated to be approximately  $2.2 \times 10^4 \times (\text{Power/GW}) \times (\text{Mass/ton}) / (\text{Baseline/m})^2$ .

### III. TEST OF NEW PHYSICS

The distinctive 3.685 MeV photon from the de-excitation of  ${}^{13}\text{C}$  provides a new avenue for testing scenarios of BSM as an explanation for the 5 MeV bump. In this section, we demonstrate how the  ${}^{13}\text{C}$  NC signal can act as a powerful tool to distinguish BSM explanations of the 5-MeV bump from potential modifications in the flux or IBD systematics. This analysis utilizes the existing NEOS data, even with the current level of background rejection provided by the experimental collaboration [41]. The primary source of background is muon-induced events. A detailed discussion of the various background sources is presented in the appendix.

As a reference model, we consider the only BSM scenario proposed so far to explain the 5-MeV bump: sterile neutrino scattering with  ${}^{13}\text{C}$ , producing a neutron and  ${}^{12}\text{C}^*$  in its first excited state ( $\nu_s + {}^{13}\text{C} \rightarrow \nu_s + n + {}^{12}\text{C}^*$ ) via the exchange of a new light gauge boson from the Lagrangian

$$\mathcal{L} = g_X X_\mu (Y_\nu \bar{\nu}_s \gamma^\mu \nu_s + \bar{p} \gamma^\mu p + Y_n \bar{n} \gamma^\mu n), \quad (2)$$

where  $g_X$  is the coupling constant of the new gauge symmetry  $U(1)_X$  with  $Y_\nu$  and  $Y_n$  being the charges of the sterile neutrino and neutron, respectively, in units of  $g_X$ . The  ${}^{12}\text{C}^*$  subsequently decays through  ${}^{12}\text{C}^* \rightarrow {}^{12}\text{C} + \gamma$  (4.4 MeV), mimicking the IBD signal [23]. Interestingly, this sterile neutrino scattering with  ${}^{13}\text{C}$  can also produce our signal:  $\nu_s + {}^{13}\text{C} \rightarrow \nu_s + {}^{13}\text{C}^*$  accompanied by  ${}^{13}\text{C}^* \rightarrow {}^{13}\text{C} + \gamma$  (3.685 MeV).

We first display the preferred parameter space explaining the 5 MeV bump in the RENO and NEOS experiments [15, 17] by the sterile neutrino scenario producing  $n + {}^{12}\text{C}^*$  following the rough estimations in Ref. [23]. The cross section of the sterile neutrino scattering with  ${}^{13}\text{C}$  is expressed as

$$\sigma_{\text{NP}} = 4\pi A_0(E) \zeta^2 \sigma_{\text{Mott}}, \quad (3)$$

where  $A_0(E)$  is an experimentally determined function of the energy transferred to the nuclear system. The Mott

cross section,  $\sigma_{\text{Mott}}$ , is given by

$$\sigma_{\text{Mott}} = \frac{\pi\alpha^2 Z^2}{E_i E_f} \left[ \log \left( \frac{4E_i E_f + M_X^2}{M_X^2} \right) - \frac{4E_i E_f}{4E_i E_f + M_X^2} \right], \quad (4)$$

where  $E_i$  is the initial-state electron energy,  $E_f = E_i - E_n - E_{\text{th}}$  is the final-state electron energy, and  $E_{\text{th}}$  is the reaction threshold energy. The term  $\zeta$  is defined as

$$\zeta = Y_\nu \left( 1 + \frac{7}{6} Y_n \right) \left( \frac{g_X^2}{e^2} \right) \sin \left( \frac{\Delta m_{41}^2 L}{4E_\nu} \right) \sin 2\theta_{ee}, \quad (5)$$

where  $\Delta m_{41}^2$  is the new mass-squared splitting and  $\theta_{ee}$  is the new mixing angle. The  $U(1)_X$  couplings for the 5 MeV bump imposed in Ref. [23] are  $Y_\nu = +10$ ,  $Y_n = -0.65$ , and  $\sin^2 2\theta_{ee} = 0.04$ . The oscillation part can be taken to be a averaged value as  $\sin^2 \left( \frac{\Delta m_{41}^2 L}{4E_\nu} \right) \rightarrow \frac{1}{2}$ .

The parameter region of the  $U(1)_X$  gauge boson mass,  $M_X$ , and the coupling  $g_X$  explaining the 5 MeV bump observed in the RENO and NEOS experiments [15, 17] with 99% C.L. are shown in Fig. 2. Our analysis is consistent with the results of Ref. [23] targeted at Daya Bay with 99% confidence. Since this scenario partially can be tested from the COHERENT experiment, the current limit is shown with black solid line following Ref. [23] in the figure, strongly constraining the parameter region for  $M_X \gtrsim 0.5$  MeV and  $g_X \gtrsim 10^{-3}$ .

As stated previously, the exactly same sterile neutrino scattering with  $^{13}\text{C}$  can also produce our signal,  $^{13}\text{C}^* \rightarrow ^{13}\text{C} + \gamma$  (3.685 MeV), which is expected to leave a sharp 3.685 MeV peak in the photon data in the reactor experiments. Here, we demonstrate that the remaining parameter space for the sterile neutrino explanation of the 5-MeV bump, as shown in Fig. 2, can be entirely excluded using the current NEOS experimental data, with the existing background subtraction provided by the experimental collaboration. In the first-order approximation, the cross section of the sterile neutrino scattering with  $^{13}\text{C}$  producing the 3.685 MeV photon can be expressed by replacing the Fermi constant,  $G_F$ , with

$$\frac{\zeta^2}{(p^2 - m_X^2) + \Gamma_X^2}, \quad (6)$$

where  $p \approx Q = 3.685$  MeV and  $\Gamma_X = \frac{g_X^2 m_X}{24\pi}$ .

Applying the current NEOS data after 180 days of data collection [41] and considering only the muon veto without discrimination between photons and other particles (such as electrons, positrons, and neutrons) in the energy window of  $3.685 \pm 0.1$  MeV, the 99% current upper bound on this scenario is represented by the solid green curve in Fig. 2. This result completely excludes the possibility of the new physics scenario explaining the 5 MeV bump proposed in Ref. [23] with more than 99% confidence even with the current data. This is due to the fact that the sterile neutrino NSI contribution to the inelastic  $\bar{\nu}_e - ^{13}\text{C}$  scattering is at least million times larger than the

SM process via  $Z$  boson exchange. Assuming 10 years of data collection without particle discrimination, the 99% upper bound is represented by the dot-dashed curve. It is possible to substantially enhance NEOS's capability to probe new physics scenarios by reducing the backgrounds to the level comparable to the number of signals, as illustrated by the dashed and dotted curves representing 180 days and 10 years of data collection, respectively. Reduction of muon and neutron backgrounds, combined with enhanced discrimination between photons and electrons/positrons, can achieve a signal-to-background ratio of a comparable order. A more detailed explanation of background reduction is provided in the appendix. Although focused on a specific sterile neutrino scenario here, our result demonstrates that any new physics scenario proposed to explain the 5-MeV bump must be consistent with the ( $^{13}\text{C}$ ) de-excitation signal, which is a critical point to emphasize.

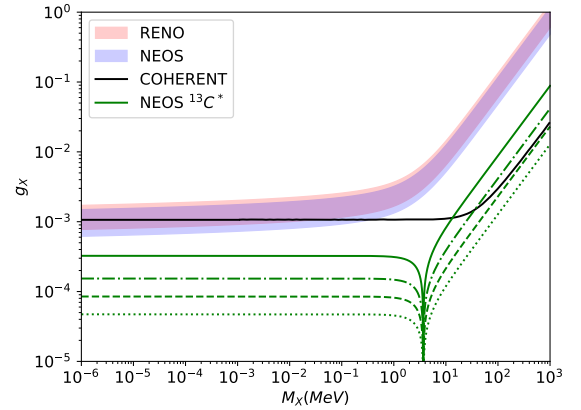


FIG. 2. 99% C.L. contour plots explaining the 5-MeV bump observed in the RENO and NEOS experiments, assuming sterile neutrinos interact with protons and neutrons via a vector boson  $X$ . The latest NEOS results, derived from 180 days of data collection using only a muon veto without particle identification, exclude this scenario at the 99% C.L., as indicated by the solid green curve based on the  $^{13}\text{C}$  NC signal. The dotted-dashed, dashed, and dotted green curves correspond to 10 years of data collection without particle discrimination, 180 days, and 10 years of data collection assuming signal and background are of the same order, respectively. The 99% C.L. constraint from COHERENT is shown by the black solid curve.

#### IV. CROSS SECTION MEASUREMENT

Because of the results discussed in Sec. III, we can more focus on the effect of reactor flux models on the 5 MeV bump. To effectively discriminate between reactor flux models, it is essential to reduce systematic uncertainties, achieve high statistics, and minimize background interference. Among the primary sources of systematic un-

certainty, cross-section uncertainty is a significant challenge. In this section, we will, for the first time, investigate  $^{13}\text{C}$  cross-section measurements using data from various experiments. This alignment is necessary to enable the discrimination of reactor flux models to evaluate the sensitivity of  $^{13}\text{C}$ .

In this section, we present our novel approach to NC  $^{13}\text{C}$  cross-section measurement, with the detection of  $^8\text{B}$  solar neutrinos at the ongoing JUNO experiment, the proposed pion and muon decay at rest ( $\pi$  DAR and  $\mu$  DAR) experiments, and isotope decay at rest (IsoDAR) which is achieved here for the first time. We briefly outline these three approaches in the following. Moreover, we will explain how reducing the cross-section uncertainty can improve the sensitivity to distinguish among reactor models and, consequently, revisit the 5-MeV bump.

The cross-section for the neutral current (NC) interaction of neutrinos with  $^{13}\text{C}$ , resulting in the production of excited  $^{13}\text{C}^*$  nuclei, is given in Eq. (1). Although not experimentally measured yet, we expect that the above theoretical calculation from nuclear physics can have about 10% level uncertainty. It has been suggested that ab initio nuclear structure calculations, incorporating chiral three-nucleon interactions and considering results from LSND, Super Kamiokande, and other neutrino experiments, could reduce the uncertainties in the neutrino- $^{12}\text{C}$  cross section to the one-percent level [30]. Building on this analysis, the JUNO collaboration in Ref. [31] proposes that  $^{13}\text{C}$  interactions could offer promising opportunities for measuring the  $^8\text{B}$  solar neutrino flux, leveraging such precise theoretical uncertainties. It should be noted, however, that our analysis is independent of the aforementioned proposal.

According to the proposals for observing the solar neutrino flux via the  $^{13}\text{C}$  NC interaction [31–33], we expect cross-section measurements to be feasible in the near future. Moreover, neutrino production from  $\pi$  DAR and  $\mu$  DAR in experiments such as LSND [42], JSNS<sup>2</sup> [43], and the proposed OscSNS [44], will provide further data. Based on the data-taking volume similar to that of LSND, we expect approximately 13 events of  $^{13}\text{C}$  excitation from neutrinos produced via pion decay at rest (with a monochromatic energy of 30 MeV), and 40 events from neutrinos can be produced via muon decay at rest, in LSND experiment. JSNS<sup>2</sup> is expected to collect a number of events comparable to those observed by LSND. Using 886 tons of mineral oil and a total neutrino flux at the OscSNS detector of  $1.64 \times 10^{14} \nu/(\text{year} \cdot \text{cm}^2)$ , and assuming three years of data collection, we anticipate collecting events at a rate twenty times higher than what was observed in the LSND experiment.

Considering  $\pi$  DAR and  $\mu$  DAR, by few ten MeV energy the cross-section becomes sensitive predominantly to the  $a_2$  term of Eq. (1). The  $a_1$  term is negligible, accounting for less than 0.3% of the total cross section. Assuming theoretical uncertainty of 10% for both  $a_1$  and  $a_2$ , the effect of  $a_1$  on the total cross-section uncertainty is

approximately 0.2% in the case of reactor neutrinos with energy range below  $\lesssim 10$  MeV. Furthermore, a combination of lower-energy neutrinos from solar and isotope decay at rest sources with higher-energy neutrinos from pion and muon decay at rest could help constrain the cubic term  $a_3$ , which is theoretically set to zero, as well as higher-order terms.

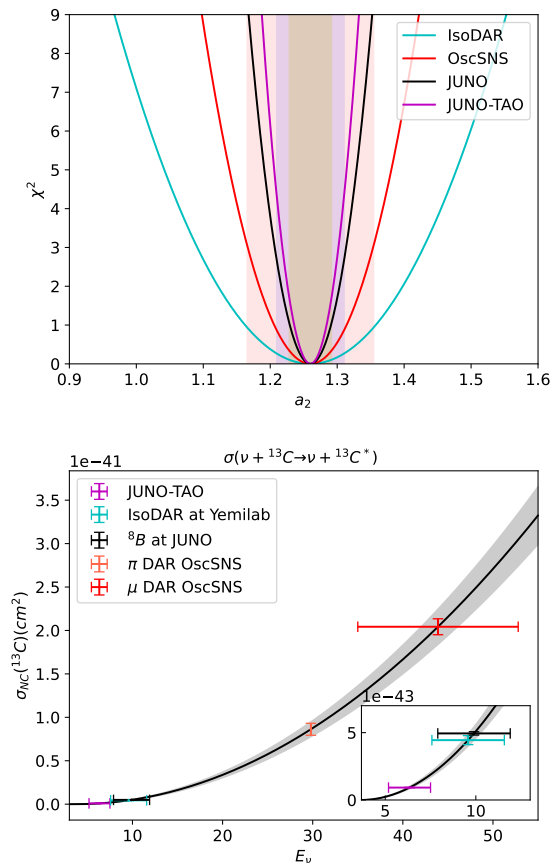


FIG. 3. The up panel shows the  $\chi^2$  as a function of the quadratic term constant  $a_2$  in Eq. (1) for different experiments, with 2.5%, 4%, and 7.5% precision measurements indicated by the shaded grey, blue, and pink regions, respectively, corresponds to JUNO, OscSNS and IsoDAR precision at  $1\sigma$ . The lower panel displays the cross section as a function of neutrino energy for JUNO-TAO, IsoDAR at Yemilab, JUNO, and pion/muon decay-at-rest experiments.

Sensitivity studies from solar neutrino experiments like JUNO, reactor experiments like JUNO-TAO, over ten years of data-taking, OscSNS pion/muon decay at rest experiment and isotope decay at rest (IsoDAR) at Yemilab, are illustrated in Fig. 3. Based on our studies in the main text, we optimistically consider the signal-to-background ratios of 20/1 for JUNO-TAO, 3/1 for JUNO, 1/1 for OscSNS, and 1/1 for IsoDAR at Yemilab, as will be explained later. For JUNO and JUNO-TAO, neglecting the background, collecting more than 3000 events, each experiment can achieve better than 2%

sensitivity in measuring the cross-section independently. For the case of OscSNS, collecting one thousand of events, measure the cross-section better than 3%. Taking the background into account, the precision of JUNO and OscSNS is 2.5% and 4%, respectively. Notably, these projections only account for statistical uncertainties in the cross-section measurement. In the lower panel of Fig. 3. We have shown the measured value of cross section with respect to the energy for our reference experiments. As follow, we will explain the sensitivity of each experiment with more details.

It is expected that JUNO solar neutrino data (300 NC  $^{13}\text{C}$  events per year) can provide precise measurement of the cross section. The main sources of background are  $\nu$ -e scattering, environmental background from radioactive isotopes, reactor events, and  $\nu_e\text{CC}$  interactions. Assuming a 95%  $\gamma/\beta$  discrimination and a 3% energy resolution, we expect that  $\nu$ -e scattering is the most significant background source, contributing approximately half of the total background events. We estimate the number of background events to be one-third of the signal. The current measurement of the  $^8\text{B}$  flux uncertainty is 3.5% from the Sudbury Neutrino Observatory (SNO) [45]. By enhancing the precision of solar neutrino oscillation parameters  $\Delta m_{21}^2$  and  $\theta_{12}$  to the sub-percent level through reactor experiments like JUNO and the LSC at Yemilab, along with the detection of pp,  $^7\text{Be}$ , and pep solar neutrinos in the LSC at Yemilab and/or Jinping, as well as  $^7\text{Be}$  neutrinos at JUNO, the precision of  $\theta_{12}$  can be improved to below 1% [8]. JUNO will detect  $^8\text{B}$  neutrinos through neutrino-electron scattering, as well as charged-current and neutral-current interactions with  $^{13}\text{C}$  nuclei [31].

On the other hand, the proposed Hyper-Kamiokande (HK) experiment will detect  $^8\text{B}$  neutrinos via neutrino-electron scattering [46], while DUNE will detect  $^8\text{B}$  neutrinos through both charged-current interactions and neutrino-electron scattering [47, 48]. There is also potential for detecting  $^8\text{B}$  neutrinos through the NC interaction with argon nuclei, though the nuclear structure of argon remains uncertain and further investigation is needed. Additionally, other proposals like the lithium-doped detector THEIA aim to detect  $^8\text{B}$  neutrinos using both charged-current interactions with lithium nuclei and neutrino-electron scattering [49]. Each of these current and future experiments—JUNO, DUNE, HK, and THEIA—will collect several hundred thousand events. With oscillation parameters measured to sub-percent precision and control over other systematics, the  $^8\text{B}$  neutrino flux could also be determined to sub-percent accuracy. Furthermore, future dark matter direct detection experiments can have a potential measuring the  $^8\text{B}$  neutrino flux with a 1% precision [50] via the Coherent Elastic Neutrino-Nucleus Scattering (CE $\nu$ NS).

Consequently, future solar neutrino experiments such as JUNO are expected to measure the  $^{13}\text{C}$  cross-section with a precision of 2% to 4%, depending on the accuracy of the  $^8\text{B}$  flux measurement, other systematic uncertainties, and background reduction. The  $^8\text{B}$  solar neutrino

flux is expected to be measured with a sub-percent or 1% level precision from future experiments (via the channels other than our 3.685 MeV signal) such as JUNO, DUNE, HK, THEIA, and dark matter direct detection experiments. Consequently, we expect JUNO can measure our  $^{13}\text{C}$  cross section with a precision of 2% to 4%. Even when the optimistic background rejections are not perfectly achieved, we expect the cross section measurements can provide enough sensitivities separating at least the reactor neutrino flux observed in RENO and the expected flux from the KI/EF model around 5 MeV energy region.

In  $\pi/\mu$  DAR experiments, the flux uncertainty for LSND is approximately 10%, while OscSNS has a flux uncertainty of only 0.8%. With a total systematic uncertainty of 10% for LSND or JSNS<sup>2</sup>, these experiments offer the potential to measure the  $^{13}\text{C}$  cross section for the first time at a level of 15%, which is comparable to the current theoretical uncertainty of the cross section. However, due to poor shielding, we expect the number of background events to be more than ten times larger than the signal, which significantly reduces the sensitivity of LSND and JSNS<sup>2</sup> for cross-section measurement. Next-generation  $\pi/\mu$  DAR experiments, such as OscSNS, with 20 times larger data samples and reduced systematic uncertainties, will not only probe the LSND anomaly but also enable precise cross-section measurements, including the neutral-current (NC) cross section of  $^{13}\text{C}$ , with the best precision of 3%, assuming total background reduction. This precision depends on factors such as efficiency and background rejection. Such measurements open up the possibility of investigating the 5-MeV bump by detecting interactions of reactor neutrinos with  $^{13}\text{C}$  and measuring the  $^8\text{B}$  solar neutrino flux, independent of uncertainties in the neutrino oscillation parameters  $\theta_{12}$  and  $\Delta m_{21}^2$ . By collecting ten times more data than OscSNS With ten times more data which can be achieved by larger detector, shorter baseline and more P.O.T., it will be possible to achieve precision measurements of  $a_2$  up to 1% level, with a sample size on the order of ten thousand events.

The Liquid Scintillator Counter (LSC) at Yemilab is a 2.26-kiloton multipurpose detector capable of detecting solar neutrinos, reactor anti-neutrinos, and anti-neutrinos produced by IsoDAR. Moreover, our estimations show that considering the IsoDAR experiment at Yemilab, we expect to detect 590 neutral current  $^{13}\text{C}$  events after four years of data collection, assuming total  $1.97 \times 10^{24}$  protons on target [7, 51]. Electron antineutrino is produced at IsoDAR from high Q-value ( $Q = 16$  MeV) of beta decay of  $^8\text{Li}$ . Based on the proposals, we expect to measure the cross section with 4% (7.5%) precision assuming no background (signal-to-background is one) in the neutrino energy region of  $\mathcal{O}(10)$  MeV. Note that the number of background events can be reduced to that comparable to the signal events if 95% level  $\gamma/\beta$  separation is achievable in the IsoDAR at Yemilab [52]. In addition, we expect 34 events per year from  $^8\text{B}$  solar neutrinos at LSC at Yemilab. From the ten years



of solar data collection and four years of beam-on data (IsoDAR), the LSC at Yemilab can maximally obtain a statistical sensitivity of 3% by collecting more than 900 events. Combination of JUNO and the LSC at Yemilab, the statistical sensitivity can be reduced to 1.5%, assuming negligible background, perfect efficiency, and collection of approximately four thousand events.

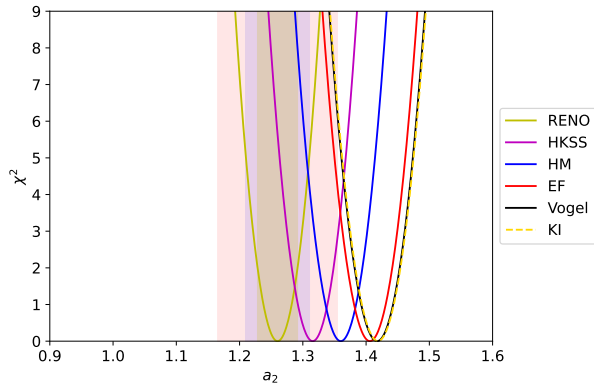


FIG. 4. The  $\chi^2$  as a function of the quadratic term constant  $a_2$  in Eq. (1) for different reactor models, using JUNO-TAO experiment. 2.5%, 4%, and 7.5% precision measurements indicated by the shaded grey, blue, and pink regions, respectively, corresponds to JUNO, OscSNS and IsoDAR presision at  $1\sigma$ .

The NC interaction of neutrino and  $^{13}\text{C}$  producing the 3.685 MeV photon can be also used to search for the supernova neutrinos. For the neutrinos from the core-collapse supernova located 10 kpc away, our estimations indicate that with all parameters consistent with those in Ref. [53], about 25 events of  $^{13}\text{C}$  can be observed at JUNO. Although this number of events is relatively small, our signal may shed light on new avenue in studying supernovae.

Measuring the cross section at three different energies—solar  $^8\text{B}$  neutrinos,  $\pi$  DAR and  $\mu$  DAR neutrinos—opens up the possibility of revisiting the 5 MeV bump observed in nuclear reactor antineutrino detection. Assuming semi-experimental flux from excess events at RENO as the true model and  $a_2 = 1.26$ , the measured values of  $a_2$  are 1.31, 1.36, 1.41, 1.42, and 1.42 for the HKSS, HM, EF, Vogel, and KI models, respectively as demonstrated in Fig. 4. The difference between the reconstructed semi-experimental flux from RENO and theoretical models ranges from 5% to 14%. However, with the expected  $1\sigma$  precision of cross-section measurements projected to be between 2.5%, 4% and 7.5% from JUNO, OscSNS and/or IsoDAR at Yemilab, would facilitate a deeper understanding of the 5-MeV bump and enhance the consistency between experimental data and theoretical predictions.

## V. FLUX MEASUREMENT SENSITIVITIES

Equipped with the reduction of systematics with cross section measurement, now we explore the flux measurement sensitivities of various experiments from the  $\bar{\nu} - ^{13}\text{C}$  NC interactions. For simplicity, we adopt the three background scenarios:  $N_{\text{background}}/N_{\text{signal}} = 6, 1$ , and 0. The first scenario assumes that all background events originate from Elastic Scattering (ES) of reactor neutrinos, with zero efficiency for  $\gamma/\beta$  separation as discussed in the appendix. This assumption, while conservative for experiments like Daya Bay and RENO, is plausible for very short baseline experiments. The second scenario is well-supported by considering effective  $\gamma/\beta$  discrimination, along with significant reductions in muon and neutron backgrounds to match the signal level. The third scenario is chosen to show the best-case scenario.

The dotted, dashed, and solid curves in Fig. 5 correspond to the  $1\sigma$  C.L. sensitivities for the first, second, and third background scenarios, respectively. The red, blue, and green curves are drawn additionally considering the systematic uncertainties of 0%, 1%, and 3%, in the given order. Note that the separation of those red, blue and green curves becomes more larger for the scenarios with smaller backgrounds. The vertical dotted lines correspond to the statistics of various past, current, and future experiments along with our new proposed detectors. For the past experiments (RENO and Daya Bay) we accounted for data collected over the entire duration of the experiment. However, for current and future experiments, we have considered 10 years of data collection. The light grey shaded region is the level of flux measurement uncertainties (4-8%) which can start to separate different theoretical flux models at  $1\sigma$ .

As can be seen in Fig. 5, the flux measurement sensitivity of RENO which could not separate photon and electron events, corresponding to our first background scenario at least (dot-dashed curves), was worse than 14%. This is definitely beyond the light grey shaded region, which means that RENO did not have sensitivity to distinguish different flux models from the  $\bar{\nu}_e - ^{13}\text{C}$  NC interactions. On the other hand, in the case of comparable signal and background, it is expected to reach about 4% sensitivity clearly distinguishing the flux models, after about 3000 events that corresponds to ten years of active running of JUNO-TAO even with the 3% level systematic uncertainty.

Now we discuss another powerful analysis method identifying the origin of the 5 MeV bump, the fission fraction evolution, which is less affected by the systematic uncertainties. As can be observed from Fig. 6, assuming fission fractions evolution in Daya Bay [54], we can distinguish various flux models by observing the time evolution of the reactor. The blue and green error bars correspond to  $1\sigma$  statistical only and statistical plus 1% systematic uncertainties respectively, assuming collection of ten thousand events. One thousand events are expected to be collected using a larger detector and a data collection

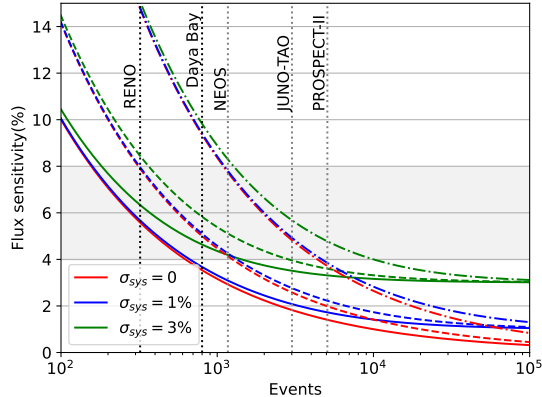


FIG. 5. Signal acceptance is universally assumed to be 100% for simplicity. The dot-dashed, dashed, and solid curves stand for our first, second, and third background scenarios, i.e.,  $N_{\text{bkg.}}/N_{\text{sig.}} = 6, 1, 0$ , respectively. For red, blue and green curves, we have considered zero, 1% and 3% systematic uncertainty respectively. The number of events of RENO and Daya Bay are from their final data while the others are from assuming ten years of data taking. The light grey shaded region (4-8%) is the level of flux measurement uncertainties that can start to separate different theoretical flux models at  $1\sigma$ .

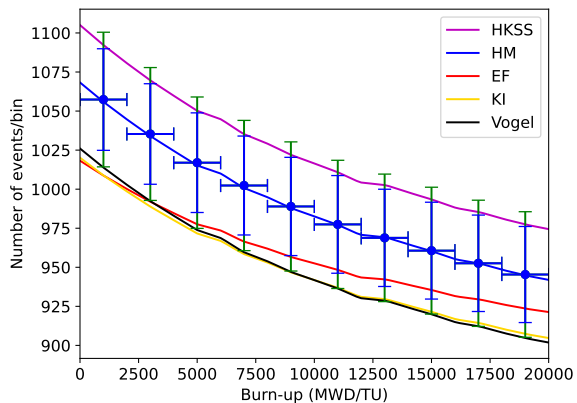


FIG. 6. Number of events versus burn up in the unit of megawatt-day over thermal unit (MWD/TU) at an experiment collection ten thousand events, considering HM as the true model.

equivalent to 100 ton-years at the NEOS site. Without considering systematics and background, it is expected to achieve a  $3.5\sigma$  sensitivity in discriminating between the HKSS and HM models. Considering 1% and 3% systematic uncertainties and including background comparable with signal, such an experiment can distinguish between HKSS and KI at  $4.5\sigma$  and  $3.5\sigma$  respectively, while it discriminate between HKSS and HM at  $2.5\sigma$  to  $1.5\sigma$ . The near future experiments JUNO-TAO and PROSPECT-II have  $3\sigma$  and  $4\sigma$  sensitivities, respectively, to distinguish

between HKSS and KI models assuming 1% systematics and neglecting the background. Moreover, under the assumption of a fixed flux model, there is a 14% difference in the number of  $^{13}\text{C}$  events between the start and end of the fuel cycle for all the demonstrated models except EF model which is 10%. This reduced rate of evolution is a sufficient discrimination between EF model and the other models. Let us emphasize that the only relevant systematic in this approach is the fission fraction systematic.

Another crucial question is how much different isotopes contribute to this bump [22]. Since the  $^{239}\text{Pu}$  fission fraction increases in time, by observing  $^{13}\text{C}$  events during fuel evolution, one can find the contribution of different isotopes to the 5 MeV bump. A steeper decrease in the number of events indicates a larger theoretical deviation from the experimental data regarding  $^{239}\text{Pu}$ . Conversely, a shallower slope suggests a greater influence of  $^{235}\text{U}$  in the observed bump. A combination of IBD and  $^{13}\text{C}$  will make it more accessible to investigate the contribution of the different isotopes to the 5 MeV bump. This indicates the potential to observe fuel evolution within a reactor, as well as to measure fission fractions during the fuel cycle or the beta spectrum ratio between  $^{235}\text{U}$  and  $^{239}\text{Pu}$ . Notice that the fission fraction of  $^{238}\text{U}$  remains nearly constant, while that of  $^{241}\text{Pu}$  exhibits a roughly linear relationship with the  $^{239}\text{Pu}$  fraction.

Measuring the evolution of reactor fuel is crucial for distinguishing between the new physics hypothesis and various flux models as explanations for the RAA or the 5 MeV bump. If it is caused by new physics effects such as sterile neutrino oscillations, then the observed deficit (RAA) or excess (5 MeV bump) should remain consistent across all fission isotopes. On the other hand, if the anomalies stem from errors in reactor modeling, one might observe variations in the deficit among different fission isotopes and the observed data would be consistent with the HKSS expectation, the magenta curve in Fig. 6. This can be achieved by comparing the event ratios observed at detectors with different baselines, or through a combination of experiments with varying baselines while considering an average neutrino energy of 6 MeV. Combining our analysis methods, both from Fig. 5 and 6, we expect that the new physics hypothesis can be tested with  $2.5\sigma$  to  $5\sigma$  level significance even with the background level  $N_{\text{background}} = N_{\text{signal}}$  and 1% systematic uncertainty.

## VI. CONCLUSION

We have revisited the origin of the 5 MeV bump using the  $^{13}\text{C}$  signal in liquid scintillators, which generates a distinctive monochromatic 3.685 MeV photon. This bump could be due to IBD systematics, new physics scenarios, or flux miscalculations. Analyzing data from NEOS, we have demonstrated that the  $^{13}\text{C}$  signal decisively rules out the only proposed BSM model explaining the 5 MeV bump with more than 99% confidence [23].



Thus, any new physics scenario must also be consistent with the constraints imposed by  $^{13}\text{C}$  interactions.

Moreover, the  $^{13}\text{C}$  signal can help differentiate between various reactor flux models, provided that the backgrounds are sufficiently reduced and systematic uncertainties are minimized. This study employs robust background reduction strategies and extensive data collection to achieve significant statistical significance.

The dominant systematic uncertainty in this context arises from the cross-section measurement. To address this, we propose for the first time leveraging the capabilities of current and future experiments, including the detection of  $^8\text{B}$  solar neutrinos at JUNO, OscSNS (a pion and muon decay-at-rest experiment), and isotope decay-at-rest experiments at Yemilab. These setups are expected to achieve cross-section uncertainties of 2.5%, 4%, and 7.5%, respectively.

With these improvements in background reduction and systematic control and by extending data-taking periods we explore the potential of current experiments to distinguish between competing flux models. Furthermore, these experiments are crucial in identifying the contributions of individual isotopes to the bump, accounting for reactor time evolution and sensitivity to fuel composition changes. Our results are crucial for addressing and resolving the persistent challenges related to reactor neutrino fluxes, as well as for exploring new physics opportunities.

## ACKNOWLEDGEMENTS

This work is supported by the Basic Research Laboratory Program of the National Research Foundation (NRF) of Korea with Grant No. RS-2022-NR070815. The work of PB, MGP, MR, and SS are additionally supported by the NRF with Grant No. NRF-2020R1I1A3072747. CSS is also supported by the NRF with Grant No. NRF-2022R1C1C1011840. CSS and SS are partly supported by IBS-R018-D1.

## Appendix A: Expected Background events

In this section, we discuss the primary sources of background for the 3.685 MeV photon signal. For a detector close to the reactor such as NEOS and its upgrade version RENE (Reactor Experiment for Neutrino and Exotics), the dominant sources are dominated by neutron- and muon-induced backgrounds. Additional backgrounds include misidentification of electrons from elastic scattering (ES) or inverse beta decay (IBD) events caused by reactor neutrinos, which scale with the signal events. Other contributions come from thallium ( $^{208}\text{Tl}$ )  $\beta$  decays due to thorium ( $^{232}\text{Th}$ ) contamination in the liquid scintillator (LS), as well as environmental backgrounds originating from external radioactivity. The contribution of  $^{13}\text{C}$  solar neutrinos is negligible for short-

baseline reactor experiments but becomes significant if  $(\text{Baseline}/\text{km})^2 \gg (\text{Power}/\text{GW})$ .

In current reactor neutrino experiments, the signal is primarily detected via inverse beta decay (IBD), which can be distinguished from other events. Consequently, moderate neutron shielding and a moderate muon veto system are sufficient for basic background reduction. However, to effectively separate the background from the  $^{13}\text{C}$  signal, more advanced background reduction techniques are needed, particularly for distinguishing between flux models or generally improving sensitivity. Nonetheless, the existing background reduction measures are sufficient for testing certain new physics scenarios, as discussed in Sec. III.

We demonstrate the feasibility of our proposal by implementing additional shielding in the currently installed one-ton RENE (Reactor Experiment for Neutrino and Exotics) detector in Korea, located 24 meters from a 2.8 GW reactor. To highlight the effectiveness of our signal, neutrino neutral current (NC) interaction with  $^{13}\text{C}$  producing a 3.685 MeV photon, we explore its potential to identify the origin of the 5-MeV bump and clarify the reactor anti-neutrino flux. We estimate the background contributions, such as neutron- and muon-induced events, and evaluate the possibility of reducing them through advanced analysis techniques or additional shielding in existing or upcoming detectors. For specificity, we focus on the RENE experiment as a concrete example.

Assuming an energy resolution of  $5\%/\sqrt{E \text{ (MeV)}}$ , we define our region of interest (ROI) as  $3.685 \text{ MeV} \pm$  the full width at half maximum (FWHM) of 0.1 MeV. For comparison, the energy resolution of JUNO-TAO is  $1\%/\sqrt{E \text{ (MeV)}}$  [60]. The current RENE detector, an upgraded version of NEOS, incorporates a gamma catcher to reduce gamma background and enhance energy resolution. The shielding for RENE consists of multiple layers: 46 cm of water, 40 cm of borated polyethylene (BPE) and high-density polyethylene (HDPE) on top, 17.5 cm of BPE and HDPE on the sides, and 7 cm of steel, 2.5 cm of lead, and 2.5 cm of aluminum. Based on simulation results [65–70], we estimate approximately  $10^6$  thermal neutron events in a one-ton detector within the deposit energy range of  $3.685 \pm 0.1 \text{ MeV}$  over one year. In the Tendon gallery, where NEOS is located and RENE will be installed, the fast neutron background is expected to result in approximately  $10^4$  events per year [64]. With a 99% photon-neutron discrimination efficiency, the number of fast neutron-induced background events is expected to be reduced to around 100 per year.

In order to reduce the thermal neutron induced backgrounds, extra shielding such as water, polyethylene, borated polyethylene, and cadmium in addition to the currently design of RENE. Photon-neutron discrimination efficiency in liquid scintillator detectors typically ranges from 90% to 99%, depending on factors such as the specific experiment, energy range, and optimization of the pulse shape discrimination (PSD) method. Notice that

the discrimination efficiency is generally higher for fast neutrons than for thermal neutrons [72]. For thermal neutrons, by adding an extra half-meter of water, with a macroscopic removal cross section for thermal neutrons of  $\Sigma_r = 0.17 \text{ cm}^{-1}$ , the thermal neutron flux is reduced by a factor of  $10^{-4}$  (since  $e^{-8.5} \approx 2 \times 10^{-4}$ ). This brings the number of thermal neutron events down to approximately 100 per year. Considering 90% to 99% photon-neutron discrimination is achievable, the expected thermal neutron background is of the order of ten to one event per year.

To reduce fast neutrons, moderators can be employed to slow them down to thermal energies. Hydrogen-rich materials, such as water, polyethylene, and paraffin, effectively slow fast neutrons through elastic scattering, as hydrogen nuclei have a mass similar to that of neutrons, enabling efficient energy transfer during collisions. Once slowed, fast neutrons can then be captured or absorbed. Neutron absorbers such as boron or cadmium are effective at capturing thermal neutrons post-moderation. High- $Z$  materials like lead, steel, and tungsten are excellent for capturing fast neutrons and also provide additional shielding against secondary gamma radiation. Overall, while thermal neutrons can be reduced using shielding and boron-doped materials, fast neutron rates can be managed and monitored through the use of extra shielding, and photon-neutron discrimination techniques.

For very short-baseline detectors with an overburden of a few tens of meters water equivalent (m.w.e.), between  $10^2$  and  $10^3$  muons pass through each square meter of the detector per second. In contrast, at sites like the RENO near detector, Daya Bay, and Double Chooz, with overburdens of several hundred m.w.e., the muon rates are significantly lower, at less than one muon per second per square meter. The current shielding for the RENE detector reduces the muon background by 60%. For NEOS, the total number of muon events in a one-ton detector is approximately  $10^7$  events per year within the energy range of  $3.685 \pm 0.1 \text{ MeV}$ . Applying the muon cut at NEOS eliminates 95% of these events within the specified energy range. However, using advanced active veto systems and discrimination techniques, such as those employed by Borexino, more than 99.99% of muons can be effectively rejected [73]. In the Borexino experiment, the cosmogenic muon background is mitigated using a combination of an active veto system and muon-electron discrimination based on scintillation and Cherenkov light. However, since the primary 3.685 MeV photon does not directly produce Cherenkov light (unless secondary charged particles are involved), better discrimination between cosmogenic muon-induced backgrounds and 3.685 MeV photon signals is expected in principle. Additionally, applying a magnetic field can deflect muons, further improving their discrimination from photons. By enhancing the energy resolution of the detector, improving shielding, implementing an effective muon

veto system, and employing advanced photon-muon discrimination techniques and/or a magnetic field, it is possible to reduce muon background events to the level of the signal or lower, even for very short-baseline detectors with minimal overburden.

For detectors with significant overburden, such as near and far detector halls of RENO, Daya Bay, and Double Chooz, only a few muon background events are expected per kton.year. Moreover, these experiments with larger baselines, neutron-induced backgrounds are less significant. Instead, ES becomes the dominant source of background. Adopting the neutron veto capability along with a fiducial volume cut in Ref. [59], we expect the misidentified ES events is about 6 times the signal events. For the current level reactor neutrino experiments, discrimination of photon and electron ( $\gamma/\beta$ ) in our ROI is almost impossible except for JUNO and JUNO-TAO which can have 90% level  $\gamma/\beta$  discrimination efficiency in the energy range of 1.25–1.75 MeV [57]. Also, a future detector design LiquidO is expected to achieve even better efficiency [61]. Conventionally the  $\gamma/\beta$  discrimination efficiency increases with energy thus for JUNO-TAO and future experiments we have assumed 95%  $\gamma/\beta$  discrimination [55]. For JUNO-TAO with a good energy resolution and  $\gamma/\beta$  discrimination, the number of ES and IBD misidentified background is expected to be twenty times smaller than signal [60]. Another source of background arises from misidentified IBD events, which constitute approximately 0.1% of the ES events.

Additionally, a significant source of background below 5 MeV comes from the beta decays of  $^{208}\text{Tl}$  in the  $^{232}\text{Th}$  decay chain, accompanied by simultaneous emissions of  $\alpha$  and  $\beta$ . For a liquid scintillator (LS) detector with  $^{232}\text{Th}$  contamination at the level of  $5 \times 10^{-17} \text{ g/g}$  (equivalent to KamLAND-level purity), we expect around one  $^{208}\text{Tl}$  event within the region of interest (ROI) per day in a 1 kt LS detector. However, by exploiting the coincidence between the  $\alpha$ -decay in the  $^{232}\text{Th}$  chain and the  $\beta$ -decay of  $^{208}\text{Tl}$ —a technique known as  $^{232}\text{Th}$ -series tagging—80% and 99% of this background can be rejected in KamLAND and JUNO, respectively [56, 58]. Even under a conservative assumption of 80% background rejection, the  $^{232}\text{Th}$ -related background would remain subdominant compared to the ES events.

Environmental backgrounds such as external radioactivities from detector walls and surrounding rocks also exist. However, fiducial volume cut can reduce those backgrounds to the 5% and negligible level, respectively [59]. These environmental backgrounds can be further mitigated using reactor on-off time and the  $\gamma/\beta$  discrimination.

In summary, the primary source of background for very short baseline experiments is cosmogenic muons and neutron-induced backgrounds, whereas for longer baseline experiments, such as the near and far halls of Daya Bay and RENO, the dominant background arises from electron scattering misidentification.

- \* pouya\_bakhti@jbnu.ac.kr  
† mgpark@jbnu.ac.kr  
‡ meshkat@jbnu.ac.kr  
§ csshin@cnu.ac.kr  
¶ sshin@jbnu.ac.kr
- [1] C. L. Cowan, F. Reines, F. B. Harrison, H. W. Kruse, and A. D. McGuire, *Science* **124**, 103 (1956).
  - [2] A. Gando *et al.* (KamLAND), *Phys. Rev. D* **88**, 033001 (2013), arXiv:1303.4667 [hep-ex].
  - [3] D. Adey *et al.* (Daya Bay), *Phys. Rev. Lett.* **121**, 241805 (2018), arXiv:1809.02261 [hep-ex].
  - [4] G. Bak *et al.* (RENO), *Phys. Rev. Lett.* **121**, 201801 (2018), arXiv:1806.00248 [hep-ex].
  - [5] Y. Abe *et al.* (Double Chooz), *JHEP* **10**, 086 (2014), [Erratum: *JHEP* 02, 074 (2015)], arXiv:1406.7763 [hep-ex].
  - [6] F. An *et al.* (JUNO), *J. Phys. G* **43**, 030401 (2016), arXiv:1507.05613 [physics.ins-det].
  - [7] S.-H. Seo *et al.*, (2023), arXiv:2309.13435 [hep-ex].
  - [8] P. Bakhti, M. Rajaei, S.-H. Seo, and S. Shin, *Phys. Rev. D* **109**, 095030 (2024), arXiv:2307.11582 [hep-ph].
  - [9] P. Vogel and J. Engel, *Phys. Rev. D* **39**, 3378 (1989).
  - [10] K. Schreckenbach, H. R. Faust, F. von Feilitzsch, A. A. Hahn, K. Hawerkamp, and J. L. Vuilleumier, *Phys. Lett. B* **99**, 251 (1981).
  - [11] F. Von Feilitzsch, A. A. Hahn, and K. Schreckenbach, *Phys. Lett. B* **118**, 162 (1982).
  - [12] T. A. Mueller *et al.*, *Phys. Rev. C* **83**, 054615 (2011), arXiv:1101.2663 [hep-ex].
  - [13] P. Huber, *Phys. Rev. C* **84**, 024617 (2011), [Erratum: *Phys. Rev. C* 85, 029901 (2012)], arXiv:1106.0687 [hep-ph].
  - [14] G. Mention, M. Fechner, T. Lasserre, T. A. Mueller, D. Lhuillier, M. Cribier, and A. Letourneau, *Phys. Rev. D* **83**, 073006 (2011), arXiv:1101.2755 [hep-ex].
  - [15] J. H. Choi *et al.* (RENO), *Phys. Rev. Lett.* **116**, 211801 (2016), arXiv:1511.05849 [hep-ex].
  - [16] F. P. An *et al.* (Daya Bay), *Phys. Rev. Lett.* **116**, 061801 (2016), [Erratum: *Phys. Rev. Lett.* 118, 099902 (2017)], arXiv:1508.04233 [hep-ex].
  - [17] Y. J. Ko *et al.* (NEOS), *Phys. Rev. Lett.* **118**, 121802 (2017), arXiv:1610.05134 [hep-ex].
  - [18] A. P. Serebrov *et al.*, *Phys. Rev. D* **104**, 032003 (2021), arXiv:2005.05301 [hep-ex].
  - [19] M. Danilov, PoS **ICHEP2022**, 616 (2022), arXiv:2211.01208 [hep-ex].
  - [20] H. Almazán *et al.* (STEREO), *J. Phys. G* **48**, 075107 (2021), arXiv:2010.01876 [hep-ex].
  - [21] M. Andriamirado *et al.* (PROSPECT, (PROSPECT Collaboration)\*), *Phys. Rev. Lett.* **131**, 021802 (2023), arXiv:2212.10669 [nucl-ex].
  - [22] P. Huber, *Phys. Rev. Lett.* **118**, 042502 (2017), arXiv:1609.03910 [hep-ph].
  - [23] J. M. Berryman, V. Brdar, and P. Huber, *Phys. Rev. D* **99**, 055045 (2019), arXiv:1803.08506 [hep-ph].
  - [24] A review of detection channels for reactor antineutrinos is found in Ref. [25].
  - [25] X. Qian and J.-C. Peng, *Rept. Prog. Phys.* **82**, 036201 (2019), arXiv:1801.05386 [hep-ex].
  - [26] J. B. Birks, *The theory and practice of scintillation counting: International series of monographs in electronics and instrumentation*, Vol. 27 (Elsevier, 2013).
  - [27] T. Suzuki, A. B. Balantekin, and T. Kajino, *Phys. Rev. C* **86**, 015502 (2012), arXiv:1204.4231 [nucl-th].
  - [28] M. Fukugita, Y. Kohyama, and K. Kubodera, *Phys. Lett. B* **212**, 139 (1988).
  - [29] T. Suzuki, A. B. Balantekin, T. Kajino, and S. Chiba, *J. Phys. G* **46**, 075103 (2019), arXiv:1904.11291 [nucl-th].
  - [30] B. R. Barrett, P. Navratil, and J. P. Vary, *Prog. Part. Nucl. Phys.* **69**, 131 (2013).
  - [31] J. Zhao *et al.* (JUNO), *Astrophys. J.* **965**, 122 (2024), arXiv:2210.08437 [hep-ex].
  - [32] J. Arafune, M. Fukugita, Y. Kohyama, and K. Kubodera, *Phys. Lett. B* **217**, 186 (1989).
  - [33] A. Ianni, D. Montanino, and F. L. Villante, *Phys. Lett. B* **627**, 38 (2005), arXiv:physics/0506171.
  - [34] L. Hayen, J. Kostensalo, N. Severijns, and J. Suhonen, *Phys. Rev. C* **100**, 054323 (2019), arXiv:1908.08302 [nucl-th].
  - [35] M. Estienne *et al.*, *Phys. Rev. Lett.* **123**, 022502 (2019), arXiv:1904.09358 [nucl-ex].
  - [36] V. Kopeikin, M. Skorokhvatov, and O. Titov, *Phys. Rev. D* **104**, L071301 (2021), arXiv:2103.01684 [nucl-ex].
  - [37] S. G. Yoon *et al.* (RENO), *Phys. Rev. D* **104**, L111301 (2021), arXiv:2010.14989 [hep-ex].
  - [38] C. Giunti, Y. F. Li, C. A. Ternes, and Z. Xin, *Phys. Lett. B* **829**, 137054 (2022), arXiv:2110.06820 [hep-ph].
  - [39] C. Zhang, X. Qian, and M. Fallot, *Prog. Part. Nucl. Phys.* **136**, 104106 (2024), arXiv:2310.13070 [hep-ph].
  - [40] Note that the HKSS model is introduced to fit the 5 MeV bump.
  - [41] K. Siyeon (NEOS), PoS **ICRC2017**, 1024 (2018).
  - [42] A. Aguilar *et al.* (LSND), *Phys. Rev. D* **64**, 112007 (2001), arXiv:hep-ex/0104049.
  - [43] S. Ajimura *et al.* (JSNS2), *Nucl. Instrum. Meth. A* **1014**, 165742 (2021), arXiv:2104.13169 [physics.ins-det].
  - [44] M. Elnimr *et al.* (OscSNS), in *Snowmass 2013: Snowmass on the Mississippi* (2013) arXiv:1307.7097 [physics.ins-det].
  - [45] S. N. Ahmed *et al.* (SNO), *Phys. Rev. Lett.* **92**, 181301 (2004), arXiv:nucl-ex/0309004.
  - [46] K. Abe *et al.* (Hyper-Kamiokande), (2018), arXiv:1805.04163 [physics.ins-det].
  - [47] F. Capozzi, S. W. Li, G. Zhu, and J. F. Beacom, *Phys. Rev. Lett.* **123**, 131803 (2019), arXiv:1808.08232 [hep-ph].
  - [48] P. Bakhti and A. Y. Smirnov, *Phys. Rev. D* **101**, 123031 (2020), arXiv:2001.08030 [hep-ph].
  - [49] M. Askins *et al.* (Theia), *Eur. Phys. J. C* **80**, 416 (2020), arXiv:1911.03501 [physics.ins-det].
  - [50] D. G. Cerdeño, M. Fairbairn, T. Jubb, P. A. N. Machado, A. C. Vincent, and C. Boehm, *JHEP* **05**, 118 (2016), [Erratum: *JHEP* 09, 048 (2016)], arXiv:1604.01025 [hep-ph].
  - [51] J. Alonso *et al.*, *Phys. Rev. D* **105**, 052009 (2022), arXiv:2111.09480 [hep-ex].
  - [52] J. R. Alonso *et al.*, *JINST* **17**, P09042 (2022), arXiv:2201.10040 [physics.ins-det].
  - [53] A. Mirizzi, I. Tamborra, H.-T. Janka, N. Saviano, K. Scholberg, R. Bollig, L. Hudepohl, and S. Chakraborty, *Riv. Nuovo Cim.* **39**, 1 (2016), arXiv:1508.00785 [astro-ph.HE].

- [54] F. P. An *et al.* (Daya Bay), Chin. Phys. C **41**, 013002 (2017), arXiv:1607.05378 [hep-ex].
- [55] Note that the use of slow LS, incorporating both Cherenkov and scintillation light, makes it available to determine the direction of electrons [62]. This would also improve  $\gamma/\beta$  discrimination efficiency.
- [56] A. Abusleme *et al.* (JUNO), Chin. Phys. C **45**, 023004 (2021), arXiv:2006.11760 [hep-ex].
- [57] H. Rebber, L. Ludhova, B. S. Wonsak, and Y. Xu, JINST **16**, P01016 (2021), arXiv:2007.02687 [physics.ins-det].
- [58] T. Hachiya (KamLAND), J. Phys. Conf. Ser. **1468**, 012257 (2020).
- [59] J. M. Conrad, J. M. Link, and M. H. Shaevitz, Phys. Rev. D **71**, 073013 (2005), arXiv:hep-ex/0403048.
- [60] A. Abusleme *et al.* (JUNO), (2020), arXiv:2005.08745 [physics.ins-det].
- [61] A. Cabrera *et al.* (LiquidO), Commun. Phys. **4**, 273 (2021), arXiv:1908.02859 [physics.ins-det].
- [62] S. D. Biller, E. J. Leming, and J. L. Paton, Nucl. Instrum. Meth. A **972**, 164106 (2020), arXiv:2001.10825 [physics.ins-det].
- [63] F. Brooks, Nuclear Instruments and Methods **4**, 151 (1959).
- [64] Y. J. Ko *et al.* (NEOS), J. Korean Phys. Soc. **69**, 1651 (2016), arXiv:1610.05111 [physics.ins-det].
- [65] B. A. Heffron, Master's Thesis, University of Tennessee (2017).
- [66] B. Hackett, *DANG and the Background Characterisation of HFIR for PROSPECT*, Ph.D. thesis, Master's thesis, University of Surrey (2017).
- [67] D. Norcini, *First search for eV-scale sterile neutrinos and precision measurement of the  $^{235}\text{U}$  antineutrino spectrum with the prospect experiment*, Ph.D. thesis, Yale University (2019).
- [68] J. Ashenfelter, B. Balantekin, C. Baldenegro, H. Band, G. Barclay, C. Bass, D. Berish, N. Bowden, C. Bryan, J. Cherwinka, *et al.*, Nuclear Instruments and Methods in Physics Research Section A: Accelerators, Spectrometers, Detectors and Associated Equipment **806**, 401 (2016).
- [69] O. Kizylova, *Characterization of Time-Varying Backgrounds in the PROSPECT Experiment* (Drexel University, 2021).
- [70] W. Lee, "Hfir simulation for k neutrino symposium," (2024), accessed: 2024-09-30.
- [71] A. Cabrera, PoS **EPS-HEP2019**, 375 (2020), arXiv:1911.03686 [hep-ph].
- [72] K. Y. Jung *et al.* (NEOS-II), JINST **18**, P03003 (2023), arXiv:2211.07892 [physics.ins-det].
- [73] G. Bellini *et al.* (Borexino), JCAP **08**, 049 (2013), arXiv:1304.7381 [physics.ins-det].